AGU PUBLICATIONS

Geophysical Research Letters

RESEARCH LETTER
10.1002/2014GL059291

Key Points:
- GPS measurements following 23 October 2011 Van earthquake
- triggered slip on a fault splay from the main rupture
- the afterslip is driven mostly by coseismic stress changes

Supporting Information:
- Readme
- Figure S1
- Table S1
- Table S2

Correspondence to:
U. Dogan,
dogan@yildiz.edu.tr

Citation:
Dogan, U., D. Ö. Demir, Z. Çakir, S. Ergintav, H. Ozener, A. M. Akoğlu, S. S. Nalbant, and R. Reilinger (2014), Postseismic deformation following the M_w 7.2, 23 October 2011 Van earthquake (Turkey): Evidence for aseismic fault reactivation, *Geophys. Res. Lett.*, *41*, doi:10.1002/2014GL059291.

Received 15 JAN 2014
Accepted 17 MAR 2014
Accepted article online 19 MAR 2014

Postseismic deformation following the M_w 7.2, 23 October 2011 Van earthquake (Turkey): Evidence for aseismic fault reactivation

Ugur Dogan[1,2], Deniz Ö. Demir[1], Ziyadin Çakir[3,2], Semih Ergintav[4], Haluk Ozener[4], Ahmet M. Akoğlu[5], Süleyman S. Nalbant[2,6], and Robert Reilinger[7]

[1]Department of Geomatic Engineering, Yildiz Technical University, Istanbul, Turkey, [2]Earth and Marine Sciences Institute, TUBITAK MRC, Izmit, Turkey, [3]Department of Geology, Istanbul Technical University, Istanbul, Turkey, [4]Department of Geodesy, Kandilli Observatory and Earthquake Research Institute, Bogazici University, Istanbul, Turkey, [5]PSE Division, King Abdullah University of Science and Technology, Thuwal, Saudi Arabia, [6]Environmental Sciences Research Institute, University of Ulster, Coleraine, UK, [7]Department of Earth, Atmospheric, and Planetary Sciences, Massachusetts Institute of Technology, Cambridge, Massachusetts, USA

Abstract Geodetic measurements following the 23 October 2011, $M_w = 7.2$ Van (eastern Turkey) earthquake reveal that a fault splay on the footwall block of the coseismic thrust fault was reactivated and slipped aseismically for more than 1.5 years following the earthquake. Although long-lasting aseismic slip on coseismic ruptures has been documented following many large earthquakes, long-lasting, triggered slip on neighboring faults that did not rupture during the earthquake has not been reported previously. Elastic dislocation and Coulomb stress modeling indicate that the postseismic deformation can be adequately explained by shallow slip on both the coseismic and splay fault and is likely driven mostly by coseismic stress changes. Thus, the slip deficit on the shallow section of the coseismic fault indicated by interferometric synthetic aperture radar-based models has been partially filled by aseismic slip, suggesting a lower likelihood for a large earthquake on the shallow section of the Van fault than suggested by previous studies.

1. Introduction

On 23 October 2011, an M_w 7.2 earthquake occurred in eastern Turkey, causing more than 600 deaths and heavy damage in the city of Van and town of Erciş (Figure 1). A large aftershock ($M_w = 5.6$) struck the city 17 days later, killing an additional 40 people. The 2011 Van earthquake is among the largest events to occur over the last 35 years in eastern Turkey. It occurred in the tectonically complex region located within the Turkish-Iranian Plateau (TIP) that formed as a result of the Arabia-Eurasia continental collision since the early Miocene (~15 Ma) [e.g., *McKenzie*, 1972; *McQuarrie et al.*, 2003] (Figure 1). The overall N-S convergence of Arabia with Eurasia at ~23 mm/yr at the location of the TIP is currently accommodated by NE-SW trending left-lateral and NW-SE trending right lateral strike-slip faults, and fewer E-W striking thrust faults [e.g., *Şengör et al.*, 1985; *Reilinger et al.*, 2006].

Although a clear and prominent surface rupture was not observed in the field after the earthquake, a fault between Lake Erçek and Lake Van (here named the Van fault) was mapped as the causative fault based on coseismic synthetic aperture radar (SAR) interferograms (at http://supersites.earthobservations.org) and some compressional surface deformation features observed along its western section [*Emre et al.*, 2011; *Dogan and Karakaş*, 2013]. Focal mechanism solutions for the main shock, the distribution of aftershocks and a number of interferometric synthetic aperture radar (InSAR) studies confirm that the earthquake took place on a ENE striking, 45°–55° NW dipping reverse fault with a minor left-lateral component, consistent with the trend and location of the Van fault [*Irmak et al.*, 2012; *Akoğlu et al.*, 2013; *Elliott et al.*, 2013; *Fielding et al.*, 2013].

Modeling of seismic waves and InSAR data reveals that coseismic slip was unusually deep and largely confined to below 10 km [*Elliott et al.*, 2013]. Analysis of early postseismic Constellation of small Satellites for the Mediterranean basin Observation (COSMO-SkyMed) (23 October 2011 to 26 October 2011) and Envisat (19 November 2011 to 19 December 2011) interferograms showed insignificant and fairly superficial afterslip.

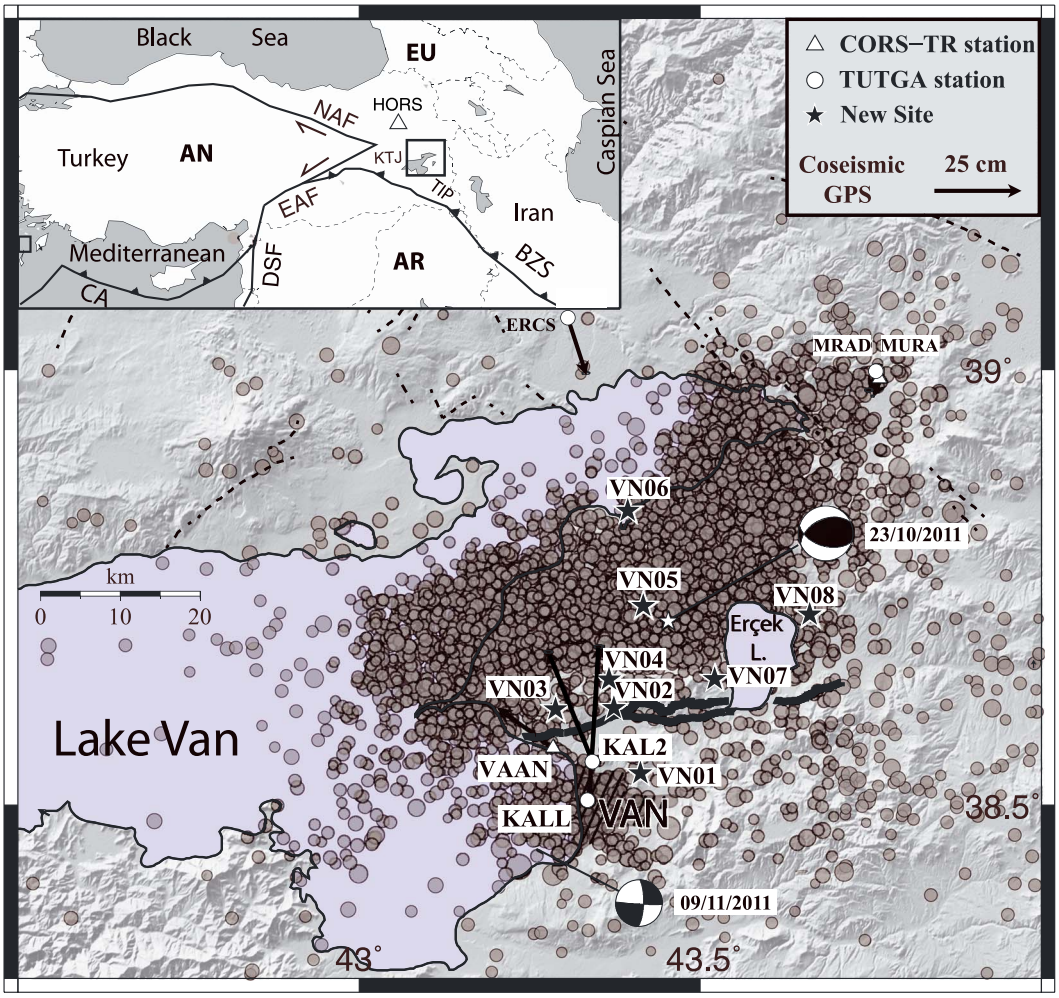

Figure 1. Tectonic map of Van and surrounding regions with active faults (dashed lines from *Şaroğlu et al.* [1992]) and proposed surface rupture (thick black lines from *Emre et al.* [2011]) for the 2011 Van earthquake on a shaded elevation image (from SRTM 90 m data). Gray circles are the aftershocks within about 6 months after the earthquake (http://udim.koeri.boun.edu.tr/). Vectors indicate the coseismic horizontal GPS displacements estimated in this study. Inset map shows major tectonic plates (AN: Anatolia, EU: Eurasia, and AR: Arabia), boundary faults in Middle East (NAF: North Anatolian Fault, EAF: East Anatolian Fault, DSF: Dead Sea Fault, CA: Cyprus Arc, BZS: Bitlis-Zagros Suture, and KTJ: Karlıova Triple Junction), and the location of the continuous GPS station (HORS located at 42.1673°N, 40.0416°E) used as reference for the coseismic and postseismic GPS displacements.

Based on the small coseismic and early postseismic shallow slip, *Elliott et al.* [2013] suggested that the shallow coseismic slip deficit could result in another damaging earthquake close to the city of Van. In contrast, as we show below, significant afterslip occurred on both the Van rupture plane and on a splay fault over 1.5 years following the main shock, which likely reduces the probability and/or magnitude of any potential earthquake on the Van fault in the aftermath of the 2011 event.

2. GPS Processing and Results

Six days after the 2011 earthquake, we visited the Van region in order to estimate coseismic displacements of existing GPS sites in the earthquake zone. Eleven sites were reoccupied and measured in static mode for 8–10 h. Coseismic offsets for six sites located within a distance of 40 km from the earthquake epicenter are shown in Figure 1. Unfortunately, there were no GPS sites on the hanging block close to the fault prior to the earthquake, although three sites were located immediately south of the rupture on the footwall block.

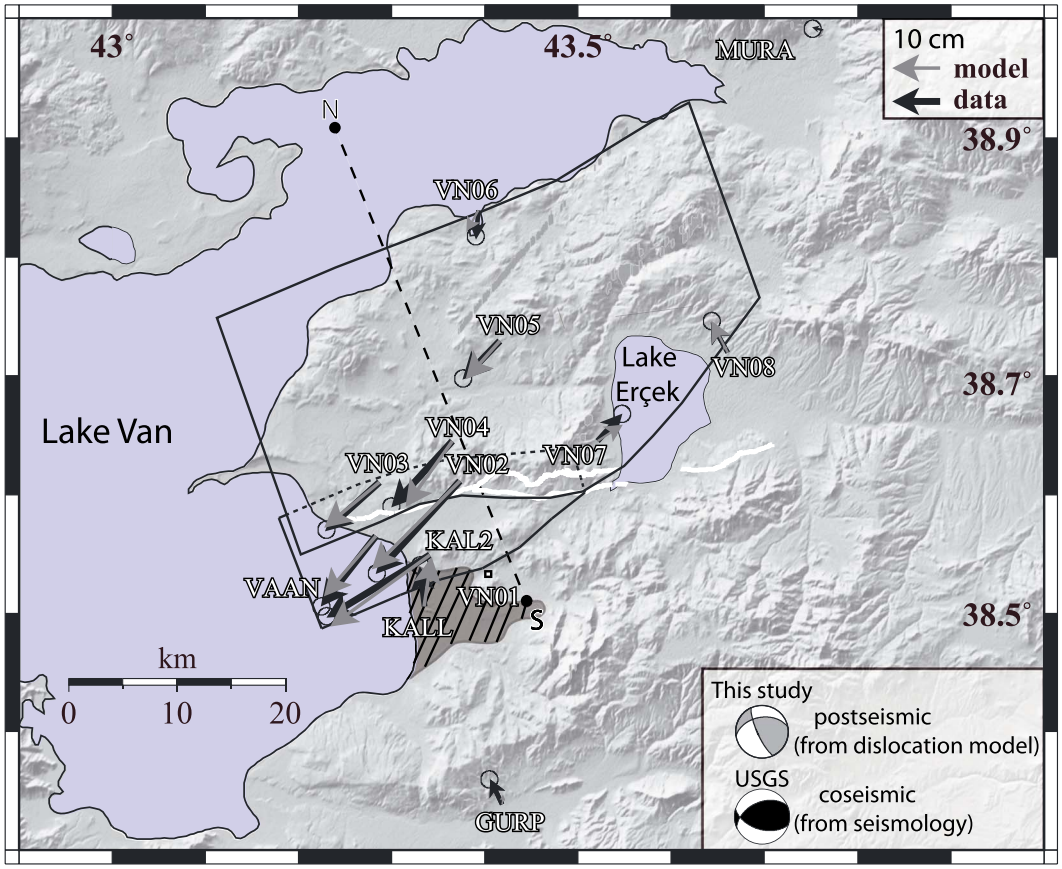

Figure 2. Observed (black) and modeled (gray) postseismic horizontal displacement vectors deduced from GPS measurements between 29 November 2011 and 20 May 2013 and their 95% confidence ellipses. Black polygons show the surface projection of the modeled fault surfaces. White lines show the surface trace of the fault thought to have been ruptured during the earthquake. The gray beach ball is the geodetic focal mechanism deduced from dislocation modeling of the postseismic GPS data using the mean fault rake and strike. It shows much more left-lateral strike-slip motion compared to the coseismic focal mechanism shown in black.

About a month after the earthquake in November 2011, we revisited the region and established eight new GPS survey sites mostly on the hanging block of the Van fault in order to monitor postseismic surface displacements (Figure 2). One of the sites (VN01) on the footwall block to the northwest of the city of Van was destroyed after the second survey. During the 1.5 year period following the earthquake, these new and the preexisting GPS sites were resurveyed 4 times (January 2012, June 2012, September 2012, and May 2013).

The GPS data were analyzed using Bernese (v5.0) software [*Dach et al.*, 2007]. We used International GNSS Service final precise ephemeris and Earth rotation parameters for the processing. Detection and repair of cycle slips were performed simultaneously for L1 and L2 phase data at triple and double difference levels. The first-degree ionospheric refraction was reduced by the ionosphere-free linear combination (L3) for double difference phase observations. The Quasi-Iono-Free Strategy was used to determine L1/L2 phase ambiguity resolution. The ionosphere-free linear combination was used for the final baseline solution using the solved L1/L2 phase integer ambiguity resolution and an atmospheric model [*Saastamoinen*, 1972] for the estimation of path delay. The troposphere zenith delays were estimated from the observations with 2 h intervals.

Estimated coseismic GPS site offsets are shown in Figure 1 (Table S1). Observed northward coseismic displacements up to 50 cm in and around the metropolitan area of Van city (site KALL) are consistent with thrust faulting on a northward dipping fault plane as interpreted from the coseismic focal mechanism

(e.g., U.S. Geological Survey Earthquake Center; Figure 2), field observations [*Emre et al.*, 2011], and InSAR studies [*Akoğlu et al.*, 2013].

Postseismic displacements were calculated, with respect to the HORS station that is located ~200 km north of the earthquake area (see inset in Figure 1), by fixing the International Terrestrial Reference Frame 2008.0, epoch 2011 coordinates of the HORS station (Table S2). To isolate postseismic deformation, the interseismic component of the site velocity was determined from pre-earthquake observations where available and otherwise estimated from the block model of *Reilinger et al.* [2006] and removed from the total measured displacements. One and a half years of horizontal postseismic displacements following the Van earthquake are listed in Table S2 and shown with black vectors in Figure 2. Except for KALL, all the sites on the western side of the fault show southwest directed horizontal motion reaching a maximum of ~26 cm at site VN02 on the hanging block immediately north of the Van fault. Pointing in the opposite direction, site VN07 on the eastern part of the fault reveals a divergent pattern of horizontal displacement at the surface consistent with blind thrust faulting. Site VN08 displays northward motion since the first measurements, suggesting that it is on the footwall of the coseismic fault, and hence, the coseismic rupture may veer toward the north along its eastern segment.

Comparison of coseismic and postseismic horizontal displacements reveals a remarkable change in the direction of motions at GPS site KAL2 and the VAAN continuous station, both located on the footwall block of the rupture plane (Figures 1 and 2). Both sites moved northward coseismically and southwestward postseismically. In contrast, other nearby GPS sites on the footwall block (i.e., KALL and GURP) show northward directed postseismic motions as expected for afterslip on the coseismic fault. We suggest that the change in the direction of postseismic motion is due to aseismic reactivation of a low-angle fault splay that runs between KALL and KAL2 north of VN01 merging with the Van fault at depth (Figures 2 and 3). This inference is supported by postseismic InSAR observations as shown in Figure 3c and 3d, and the logarithmic decay of postearthquake motion of the VAAN site (Figure 4). Tracing the phase discontinuity reveals a 20 km long splay (named here the Bostaniçi fault) that passes through the northern part of the city and reaches the railway port by Lake Van. Although the Bostaniçi fault follows the foothills north of the city, its topographic expression is not clear in the city center on the alluvial plain. The time series for the motion of site KAL2 with respect to site KALL, bracketing the Bostaniçi fault, indicates a logarithmic rate decrease between these sites, consistent with postseismic relaxation processes on the Bostaniçi fault. The time series of continuous GPS site VAAN, also characterized with a logarithmic relaxation function, suggests that aseismic creep will likely continue (Figure 4). Analysis of the motion of site KAL2 with respect to other sites on the hanging wall (e.g., VN02) reveals similar temporal decays on the Bostaniçi and Van faults.

3. Modeling

The temporal and spatial patterns of postseismic deformation are consistent with triggered aseismic slip both on the coseismic rupture plane and its southern splay. To investigate this further, we use the Poly3Dinv inversion software [*Maerten et al.*, 2005] to estimate the cumulative postseismic slip observed between 1 month and 1.5 years following the earthquake. The Poly3D method is based on the analytical solution for a triangular dislocation in a linear, elastic, homogeneous, and isotropic half space, which uses triangular surfaces as discontinuities [*Thomas*, 1993]. The use of triangular elements allows us to construct fault models that better approximate 3-D fault surfaces, avoiding gaps and overlaps that are inevitably encountered when modeling a complex network of faults with simple rectangular dislocations. A coseismic rupture surface 50 km long and 28 km wide was constructed with a northward dip of ~50° inferred from InSAR data [*Akoğlu et al.*, 2013] using triangular elements of about 4×4 km in dimension along the dip and strike directions. The location and strike of the eastern part of the coseismic fault could not be well determined due to Lake Erçek. Coseismic Envisat interferograms [*Elliott et al.*, 2013] and the postseismic displacement of site VN08 suggest that the rupture likely runs northeast through the lake. Future measurements on a new site established in September 2013 south of the Lake Erçek may provide better constraints on the eastern extension of the fault. The surface trace of the Bostaniçi fault was located based on postseismic interferograms as shown in Figures 3c and 3d. We assume that the two faults merge at depth (Figure 3b). Modeling tests show that the goodness of fit increases nearly linearly with decreasing depth (i.e., with decreasing fault dip), precluding

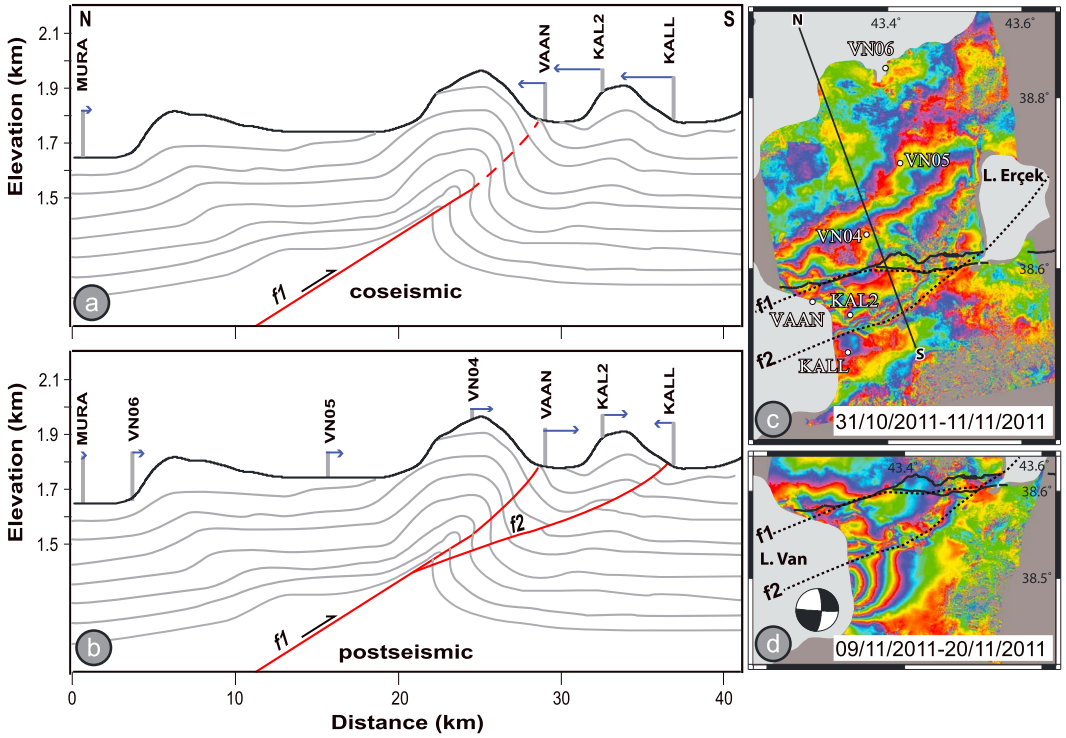

Figure 3. Relationship between (a) coseismic and (b) postseismic deformation illustrated with schematic geological cross sections with real topography along the N-S profile shown in Figures 2 and 3c. Blind slip on coseismic fault (f1; Van fault) causes all the GPS sites on the footwall block to move northward (Figure 3a). During the postseismic period, in addition to the shallow section of the fault, a fault splay (f2; i.e., Bostaniçi fault) that crops out farther south beneath the coseismic fault starts slipping aseismically, reversing the direction of motion at the VAAN and KAL2 benchmarks(Figure 3b). (c, d) Evidence of aseismic deformation along the Van and Bostaniçi faults can be seen in postseismic interferograms with 10 days temporal baselines we constructed from a descending (Figure 3c) and ascending (Figure 3d) pair of TerraSAR-X images (data from http://supersites.earthobservations.org) using Delft Object-oriented Radar Interferometric Software InSAR processing software [*Kampes et al.*, 2003]. Solid and dotted black lines show the surface ruptures inferred from coseismic interferograms and limited ground deformation and modeled surface ruptures, respectively. Circular fringes in the metropolitan area of Van city (Figure 3d) are due to surface deformation caused by the $M_w = 5.6$, 9 November 2011 aftershock whose focal mechanism calculated by the USGS is shown with a beach ball. The difference in the fringe pattern of the aftershock between the two interferograms is due to the difference in the radar-viewing geometry. Aseismic slip along the Bostaniçi fault (f2) may be the cause of the clearly observed offsets and disturbances to the coseismic fringes of the aftershock.

determination of an optimum depth from the GPS observations (Figure 4c). We chose a dip of 30° that corresponds to a depth of 5 km (Figure 4c). The slip distribution on both faults was then inverted for with a negativity constraint on the dip slip component (i.e., no normal slip) using both horizontal and vertical components of GPS displacements (Table S1). To avoid unphysical oscillatory slip, a smoothing operator was applied to the modeled slip distribution [*Çetin et al.*, 2012]. We chose a smoothing factor of 0.25 that provides the best compromise between the roughness of slip and misfit to the data for both the Van and Bostaniçi faults (Figure 4c). This model has a weighted root-mean-square misfit of 1.27 cm and explains well the amplitude and direction of observed horizontal displacements (Figure 2). Vertical displacements fit relatively less well as they were weighed less in the inversion (Figure S1).

The final model of postseismic slip distribution (Figure 5) shows aseismic thrust slip with a significant left-lateral component particularly on the coseismic rupture, which can also be seen from the geodetic focal mechanism estimated from the simplified dislocation model (Figure 2). A minor right lateral slip component is predicted on the eastern shallow portion of the fault accounting for the eastward motion at site VN07. While the maximum slip (~50 cm) is found to be on the shallow section of the Bostaniçi fault, an elliptical lobe of afterslip reaching 40 cm is predicted to be centered at ~11 km depth on the Van rupture plane. It must be

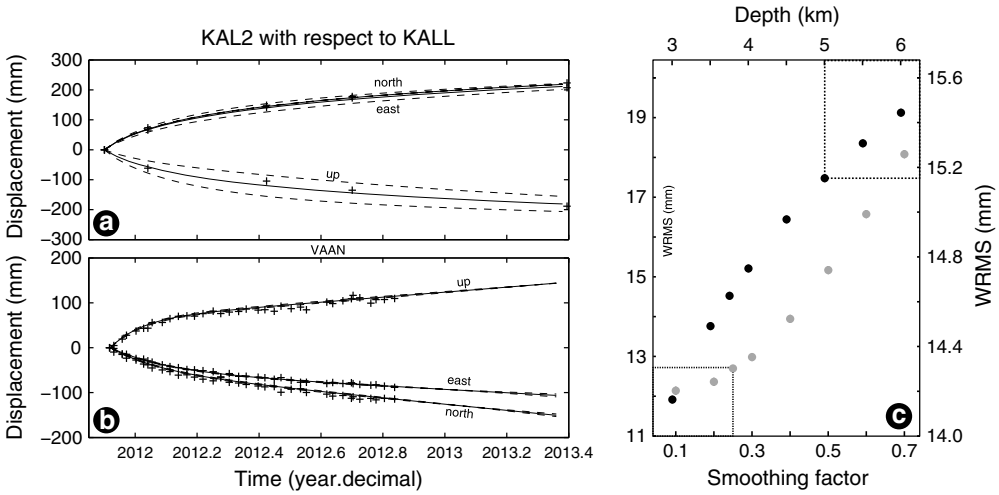

Figure 4. (a) Time series of KAL2 with respect to KALL that shows the logarithmically decreasing total displacement across the Bostaniçi fault indicative of postseismic fault slip (Figure 2). Measurements of these sites were conducted after the 9 November 2011 aftershock. (b) Time series of VAAN continuous GPS station. The thin curved line is a fit to the coordinate changes of the form $a + b \log(t)$ (where t is the time after the earthquake in years, a and b are constants) with dashed lines showing the 95% confidence interval [*Savage et al.*, 2005]. (c) Fitting tests of varying smoothing factors for slip distribution and depth at which the Van and Bostaniçi faults merge. The selected depth and smoothing factor are shown with dashed boxes.

noted that slip on the shallow part of the Van fault is difficult to distinguish from slip on the splay, and given the small number of stations, the resolution of some features in the model is rather limited, in particular the highly variable rake. In addition, some parts of this high-strain release on the splay and on the eastern section of the Van fault may result from lack of nearby GPS sites.

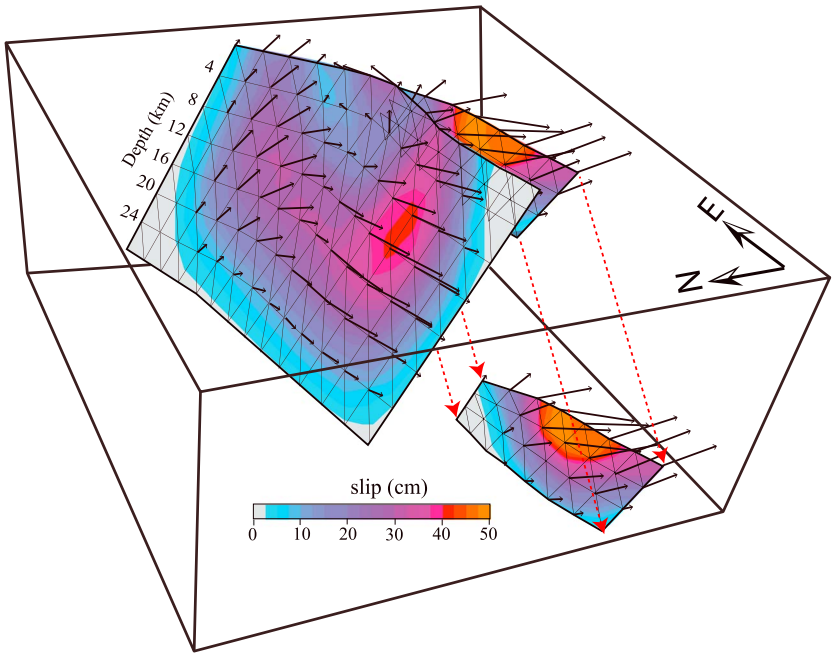

Figure 5. Block diagram showing a 3-D perspective view of the modeled Van and Bostaniçi faults with distribution of estimated postseismic slip during ~1.5 years following the earthquake. Black vectors indicate direction and amplitude of slip. Although aerially, there is a large overlap between the coseismic and postseismic slip on the main fault; large postseismic afterslip is located on the western upper parts of the main fault, a region with low or no coseismic slip (Figure S1).

4. Discussion and Conclusions

Field observations and geodetic measurements show that moderate to large earthquakes often reactivate nearby faults triggering aseismic surface slip [*Allen et al.*, 1972; *Wright et al.*, 2001; *Fialko et al.*, 2002; *Fielding et al.*, 2004; *Wei et al.*, 2011]. The Van earthquake provides an opportunity to gain further insights into triggered slip and crustal deformation along active faults. The phenomena of seismically triggered slip affect directly the rate of strain accumulation and stress on the fault and accordingly seismic hazard estimates. Static or dynamic stress or strain transfer is thought to trigger slip on preexisting, nearby, or distant faults by changing the state of stress on them [*Hill et al.*, 1993; *Stein et al.*, 1992; *King et al.*, 1994; *Nalbant et al.*, 2005] or modifying the properties of the fault zone [*Fialko et al.*, 2002]. Such transient slip events are often short-lived phenomenon occurring simultaneously or shortly after a large earthquake [*Cervelli et al.*, 2002; *Fielding et al.*, 2004]. A COSMO-SkyMed coseismic interferogram calculated using a SAR image taken only 4 h after the Van earthquake shows no clear phase discontinuity indicating triggered slip across the Bostaniçi fault [*Elliott et al.*, 2013]. Thus, the triggered slip on the Bostaniçi fault did not occur immediately at the time of the Van rupture but started some time after it and lasted more than 1.5 years. An Envisat interferogram calculated by [*Elliott et al.*, 2013, Figure S5] using images from 1 to 2 months after the main shock clearly shows deformation along the splay. A similar triggered slip may have occurred on the Berrocal thrust fault following the 1989 Loma Prieta earthquake on the San Andreas fault [*Bürgmann et al.*, 1997], but it is not known whether or not the Berrocal fault broke simultaneously during the coseismic rupture.

The causes for the delay in triggered slip are not known at the moment. However, modeling of the coseismic Coulomb stress change following the Van earthquake shows that static stress on the deeper section of the Bostaniçi fault was increased up to several MPa (Figure S1d). Combination of the stress changes due to the coseismic and postseismic slips on the Van rupture as well as fluid migration driven by coseismic strain changes might be the most likely mechanism to explain triggering and sustaining the aseismic slip on the Bostaniçi fault. Further evidence of aseismic deformation along the Van and Bostaniçi faults can be seen in postseismic interferograms with 10 days temporal baselines constructed from a descending and ascending pair of TerraSAR-X images (Figure 3d).

The total cumulative postseismic geodetic moment including both faults is 9.8×10^{18} N m which is equivalent to an $M_w = 6.6$ event or 12% of the main shock moment release (compared to U.S. Geological Survey (USGS) body wave Moment Tensor Solution). Therefore, the slip deficit on the shallow section of the coseismic fault predicted by InSAR-based models [*Elliott et al.*, 2013] is filled by a significant amount of postseismic slip, suggesting that the potential for a large earthquake on the shallow section of the Van fault may have been considerably reduced. If, as suggested by *Akoğlu et al.* [2013], the coseismic slip deficit in the upper seismogenic crust is due to the presence of ophiolitic cover rocks [*Şengör et al.*, 2008] which exhibit velocity-strengthening frictional behavior, then the seismic hazard for the city of Van will be lower than otherwise estimated. Stress transfer caused by the aseismic slip should also be taken into account in the assessments of seismic hazards for nearby seismically active faults. In addition, aseismic slip on the main or secondary fault has important implications for paleoseismic studies, particularly for those in which magnitudes of paleo-earthquakes are estimated based on surface offset measurements. Space-time evolution and the nature of the postseismic deformation will be constrained better by additional survey mode and continuous GPS measurements planned for the next 3 years.

Acknowledgments

This research was supported by the project 112Y109 of TUBITAK CAYDAG 1001 and the project 2012-05-03-KAP02 of Yildiz Technical University Scientific Research Projects Coordination Department and NSF grants 0838488 and 1321796 to MIT. GPS equipment was provided by TUBITAK MRC, Earth and Marine Research Institute. We thank Emre Havazlı, Kerem Halıcıoglu, Alpay Özdemir, Umut Ürün, and Bilal Erat for their contributions to GPS survey observations. The continuous GPS data sets were carried out in the frame of the "TUSAGA-AKTIF Project." Most figures are drawn with GMT [*Wessel and Smith*, 1998]. We thank Roland Bürgmann, Isabelle Ryder, and an anonymous reviewer for constructive comments that greatly improved this manuscript.

The Editor thanks Roland Burgmann, Isabelle Ryder, and an anonymous reviewer for their assistance in evaluating this paper.

References

Akoğlu, A. M., S. Jonsson, Z. Çakir, S. Ergintav, U. Dogan, T. Wang, B. Osmanoğlu, G. Feng, C. Zabcı, and Ö. Emre (2013), An improved source model for the *Mw* 7.1, October 23, 2011 Van (Turkey) earthquake: New insights from SAR pixel offsets and coastal uplift measurements, EGU, Vienna, Austria, 07–12 April 2013.

Allen, C. R., M. Wyss, J. N. Brune, A. Granz, and R. Wallace (1972), Displacements on the Imperial, Superstition Hills, and San Andreas faults triggered by the Borrego Mountain earthquake, *U.S. Geol. Surv. Prof. Pap.*, vol. 787, pp. 87–104, U.S. Government Printing Office, Washington, D. C.

Bürgmann, R., P. Segall, M. Lisowski, and J. L. Svarc (1997), Postseismic strain following the 1989 Loma Prieta earthquake from GPS and leveling measurements, *J. Geophys. Res.*, *102*, 4933–4955.

Cervelli, P., P. Segall, K. Johnson, M. Lisowski, and A. Miklius (2002), Sudden aseismic fault slip on the south flank of Kilauea volcano, *Nature*, *415*, 1014–1018.

Çetin, E., M. Meghraoui, Z. Çakir, A. M. Akoglu, O. Mimouni, and M. Chebbah (2012), Seven years of postseismic deformation following the 2003 *Mw* = 6.8 Zemmouri earthquake (Algeria) from InSAR time series, *Geophys. Res. Lett.*, *39*, L10307, doi:10.1029/2012GL051344.

Dach, R., U. Hugentabler, P. Fridez, and M. Meindl (2007), Bernese GPS software version 5.0, Stämpfli Publications AG, Bern, Switzerland.

Dogan, B., and A. Karakaş (2013), Geometry of co-seismic surface ruptures and tectonic meaning of the 23 October 2011 *Mw* 7.1 Van earthquake (East Anatolian Region, Turkey), *J. Struct. Geol.*, *46*, 99–114.
Elliott, J. R., A. C. Copley, R. Holley, K. Scharer, and B. Parsons (2013), The 2011 *Mw* 7.1 Van (eastern Turkey) earthquake, *J. Geophys. Res. Solid Earth*, *118*, 1–19, doi:10.1002/jgrb.50117.
Emre, O., T. Duman, S. Özalp, and H. Elmaci (2011), 23 Ekim 2011 Van depremi saha gözlemleri ve kaynak faya ilişkin ön değerlendirmeler, Tech. Rep., Mineral Research and Exploration General Directorate of Turkey, Ankara. [Available at http://www.mta.gov.tr/v2.0/deprem/2011_Van-Depremi_On-Degerlendirmeler.pdf.]
Fialko, Y., D. Sandwell, D. Agnew, M. Simons, P. Shearer, and B. Minster (2002), Deformation on nearby faults induced by the 1999 Hector Mine earthquake, *Science*, *297*, 1858–1862.
Fielding, E. J., T. J. Wright, J. Muller, B. E. Parsons, and R. Walker (2004), Aseismic deformation of a fold-and-thrust belt imaged by synthetic aperture radar interferometry near Shahdad, southeast Iran, *Geology*, *32*(7), 577–580.
Fielding, E. J., A. Sladen, Z. Li, J. P. Avouac, R. Bürgmann, and I. Ryder (2013), Kinematic fault slip evolution source models of the 2008 *M*7.9 Wenchuan earthquake in China from SAR interferometry, GPS and teleseismic analysis and implications for Longmen Shan tectonics, *Geophys. J. Int.*, *194*(2), 1138–1166, doi:10.1093/gji/ggt155.
Hill, D. P., et al. (1993), Seismicity remotely triggered by the magnitude 7.3 Landers, California, earthquake, *Science*, *260*, 1617–1622.
Irmak, T. S., B. Dogan, and A. Karakas (2012), Source mechanism of the 23 October 2011 Van (Turkey) earthquake (*Mw* = 7.1) and aftershocks with its tectonic implications, *Earth Planets Space*, *64*(11), 991–1003.
Kampes, B., R. Hanssen, and Z. Perski (2003), Radar interferometry with public domain tools, ESA Fringe Meeting, 1–5 December 2003, Frascati, Italy.
King, G. C. P., R. S. Stein, and J. Lin (1994), Static stress changes and the triggering of earthquakes, *Bull. Seismol. Soc. Am.*, *84*(3), 935–953.
Maerten, F., P. Resor, D. Pollard, and L. Maerten (2005), Inverting for slip on three-dimensional fault surfaces using angular dislocations, *Bull. Seismol. Soc. Am.*, *95*(5), 1654–1665.
McKenzie, D. P. (1972), Active tectonics of the Mediterranean region, *Geophys. J. R. Astron. Soc.*, *30*, 109–185.
McQuarrie, N., J. M. Stock, C. Verdel, and B. P. Wernicke (2003), Cenozoic evolution of the Neotethys and implications for the causes of plate motions, *Geophys. Res. Lett.*, *30*(20), 2036, doi:10.1029/2003GL017992.
Nalbant, S., S. Steacy, K. Sieh, D. Natawidjaja, and J. McCloskey (2005), Earthquake risk on the Sunda trench, *Nature*, *435*(7043), 756–757.
Reilinger, R., et al. (2006), GPS constraints on continental deformation in the Africa–Arabia–Eurasia continental collision zone and implications for the dynamics of plate interactions, *J. Geophys. Res.*, *111*, B05411, doi:10.1029/2005JB004051.
Saastamoinen, J. (1972), Introduction to practical computation of astronomical refraction, *Bull. Géod.*, *106*, 383–397.
Şaroğlu, F., Ö. Emre, and I. Kuşçu (1992), Active fault map of Turkey, General Directorate of Mineral Research and Exploration, Ankara, Turkey, 2 sheets, 1.2 000 000 scale.
Savage, J. C., J. L. Svarc, and S. B. Yu (2005), Postseismic relaxation and transient creep, *J. Geophys. Res.*, *110*, B11402, doi:10.1029/2005JB003687.
Şengör, A. M. C., N. Görür, and F. Şaroğlu (1985), Strike-slip faulting and related basin formation in zones of tectonic escape: Turkey as a case study, *Strike Slip Deformation, Basin Formation, and Sedimentation Symposium*, The Society of Economic Paleontologists and Mineralogists (SEPM) special publication, vol. 37, edited by K. T. Biddle and N. Christie Blick, pp. 227–264, Tulsa, Okla.
Şengör, A. M. C., M. S. Özeren, M. Keskin, M. Sakınç, A. D. Özbakır, and İ. Kayan (2008), Eastern Turkish high plateau as a small Turkic-type orogen: Implications for post-collisional crust-forming processes, *Earth Sci. Rev.*, *90*, 1–48.
Stein, R. S., G. C. P. King, and J. Lin (1992), Change in failure stress on the southern San Andreas Fault System caused by the 1992 magnitude = 7.4 Landers earthquake, *Science*, *258*(5086), 1328–1332.
Thomas, A. L. (1993), Poly3D: A three-dimensional, polygonal element,displacement discontinuity boundary element computer program with applications to fractures, faults, and cavities in the Earth's crust, M.S. thesis, Stanford Univ., Stanford, Calif.
Wei, M., D. Sandwell, Y. Fialko, and R. Bilham (2011), Slip on faults in the Imperial Valley triggered by the 4 April 2010 *Mw* 7.2 El Mayor-Cucapah earthquake revealed by InSAR, *Geophys. Res. Lett.*, *38*, L01308, doi:10.1029/2010GL045235.
Wessel, P., and W. H. F. Smith (1998), New, improved version of the generic mapping tools released, *EOS Trans. AGU*, *79*, 579.
Wright, T., E. Fielding, and B. Parsons (2001), Triggered slip: Observations of the 17 August 1999 Izmit (Turkey) earthquake using radar interferometry, *Geophys. Res. Lett.*, *28*, 1079–1082.